Aircraft Engine Performance Study Using Flight Data Recorder Archives

Yashovardhan S. Chati* and Hamsa Balakrishnan [†]

Massachusetts Institute of Technology, Cambridge, Massachusetts, 02139, USA

Aircraft emissions are a significant source of pollution and are closely related to engine fuel burn. The onboard Flight Data Recorder (FDR) is an accurate source of information as it logs operational aircraft data in situ. The main objective of this paper is the visualization and exploration of data from the FDR. The Airbus A330 - 223 is used to study the variation of normalized engine performance parameters with the altitude profile in all the phases of flight. A turbofan performance analysis model is employed to calculate the theoretical thrust and it is shown to be a good qualitative match to the FDR reported thrust. The operational thrust settings and the times in mode are found to differ significantly from the ICAO standard values in the LTO cycle. This difference can lead to errors in the calculation of aircraft emission inventories. This paper is the first step towards the accurate estimation of engine performance and emissions for different aircraft and engine types, given the trajectory of an aircraft.

I. Introduction

Aircraft emissions depend on engine characteristics, particularly on the fuel flow rate and the thrust. It is therefore, important to accurately assess engine performance and operational fuel burn. Traditionally, the estimation of fuel burn and emissions has been done using the ICAO Aircraft Engine Emissions Databank[1]. However, this method is approximate and the results have been shown to deviate from the measured values of emissions from aircraft in operation[2,3]. This observation has motivated the development of new approaches for fuel burn estimation[4,5]. The Flight Data Recorder (FDR) is the most accurate, onboard repository of data as it archives operational data from an aircraft. Few prior studies have made use of this data[6] and have been restricted to fuel burn estimation for specific aircraft phases, like taxi[7], or landing and takeoff operations[8].

The study presented in this paper uses FDR data from the twin - engined Airbus A330 - 223 to study the engine performance in all the phases of flight. It focuses solely on the trends observed in the engine performance data. Section II briefly describes the Flight Data Recorder (FDR). Section III describes the methodology adopted to identify the different flight phases and Section IV describes the airports encountered in the study. In Section V, the trends of various engine performance parameters are observed as a function of the altitude profile. In Section VI, an engine analysis model is used to calculate the theoretical thrust, which is then compared with the FDR reported thrust. Section VI also compares the operational thrust settings and the times in mode with the ICAO standard values for the LTO cycle. Section VII highlights the main results and gives the scope for future work. The appendix describes in detail the turbofan engine performance model used to calculate the theoretical thrust.

---

*Graduate Research Assistant, International Center for Air Transportation, Massachusetts Institute of Technology, AIAA Student Member.

†Associate Professor, Department of Aeronautics and Astronautics, Massachusetts Institute of Technology, AIAA Associate Fellow.

American Institute of Aeronautics and Astronautics

II.   Flight Data Recorder (FDR)

The Flight Data Recorder (FDR) is an instrument on board the aircraft which records the values of key flight parameters during the flight. The FDR used in our study reports 103 important parameters. However, for this study, only those parameters which are relevant for engine performance calculations are considered. FDR data from the Airbus A330 - 223 are used for all analysis. The A330 - 223 is a twin - engined turbofan aircraft, powered by the Pratt and Whitney PW 4168A/4170 engine.

III.   Flight Phase Identification

The trajectory of each flight is split into different phases. The phases are (Figure 1):

1. Departure taxi

2. Takeoff roll and wheels off

3. Ascent/Climb

4. Cruise

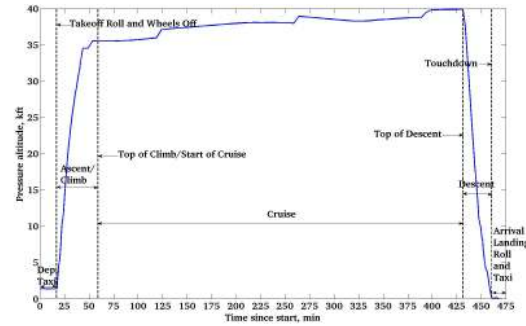5. Descent

6. Touchdown

7. Arrival landing roll and taxi

Figure 1. A330 - 223: a typical profile of the pressure altitude versus time and the different flight phases

The FDR records of aircraft trajectory parameters like latitude, longitude, pressure altitude, ground speed and their slopes are used to identify the points of transition from one flight phase to the other. The phase from the first movement of the aircraft upto the start of the takeoff roll is the departure taxi phase. The wheels - off condition is identified by the pressure altitude relative to the departure airport elevation becoming 0 and then subsequently increasing as the aircraft climbs. Climb follows, until the cruise phase. The start of cruise is identified by the leveling out of the altitude. The period of descent continues from the end of cruise until wheels - on. Touchdown is identified by the FDR reported value of the pressure altitude relative to the arrival airport elevation becoming 0. Subsequently, the entire phase till the aircraft comes to a stop is the landing roll and taxi phase. It is important to note that all the above criteria make use of just the flight trajectory information as a function of time. These criteria for flight phase identification are adopted by manual inspection of the trends in the FDR trajectory data and can be easily adjusted for other aircraft types, if required.

The time between two successive recordings of the FDR varies with the flight phase. It is 5 s during the departure taxi, and the arrival taxi phases, 1 s during takeoff, the initial part of ascent, the latter part of descent, and touchdown, 10 s during the latter part of ascent, and the initial part of descent, and 300 s during cruise.

IV.   Airports

The A330 - 223 flights included in this study operate out of six airports. Some of the key characteristics of these airports are tabulated in Table 1.

Based on their elevations Above the Mean Sea Level (AMSL), the airports are divided into three categories:

1. Sea level airports (0 – 200 ft): MIA, EWR, YUL, and DAR,

2. Mid elevation airports (around 1400 ft): ZRH, and

3. High elevation airports (around 5000 ft): NBO

American Institute of Aeronautics and Astronautics

Table 1. Airports for A330 - 223

Sr. No.	Name of the Airport	Airport Latitude	Airport Longitude	Airport Elevation (AMSL)	Length of the Longest Runway (m)
1.	Miami International Airport (MIA)	25.80°N	80.28°W	2 m (8 ft)	3962
2.	Newark Liberty International Airport (EWR)	40.69°N	74.17°W	5 m (18 ft)	3353
3.	Montréal-Pierre Elliot Trudeau International Airport (YUL)	45.46°N	73.75°W	36 m (118 ft)	3353
4.	Julius Nyerere International Airport, Dar es Salaam (DAR)	6.88°S	39.20°E	55 m (182 ft)	3000
5.	Zurich Airport (ZRH)	47.46°N	8.55°E	432 m (1416 ft)	3700
6.	Jomo Kenyatta International Airport, Nairobi (NBO)	1.32°S	36.93°E	1624 m (5327 ft)	4117

A total of 100 A330 - 223 flights are chosen for this study. Out of the 100 takeoffs, 44 are from sea level airports, 39 are from mid elevation airports, and 17 are from high elevation airports. Similarly, out of the 100 landings, 43 are to sea level airports, 41 are to mid elevation airports, and 16 are to high elevation airports.

V.   Parametric Study of Engine Performance

V.A.   Methodology

The trends of the following engine performance parameters (per engine) are studied as a function of the aircraft altitude. This study is done to facilitate visual exploration of the engine performance data from the FDR. For all flight phases except the ascent phase, the atlitude is the pressure altitude above mean sea level. For the ascent phase, the altitude is the pressure altitude relative to the AMSL elevation of the departure airport.

1. Operating Pressure Ratio (OPR)

2. Fuel flow rate

3. Engine Pressure Ratio (EPR)

4. Exhaust Gas Temperature (EGT)

5. Thrust

For the 100 A330 - 223 flights in this study, the above enumerated FDR reported parameters corresponding to the same pressure altitude (rounded to the nearest integer in feet) are collected and their average and standard deviation calculated. Since, taxi, takeoff, and landing occur at airports which have a fixed elevation, the parameters in these phases are further averaged about altitudes corresponding to the airport categories enumerated in Section IV. Specifically, the averaging is done over the altitude ranges 27 – 217 ft (for the sea level airports), 1390 – 1424 ft (for the mid elevation airports), and 5347 – 5389 ft (for the high elevation airports). For step cruise, the parameters are further averaged $\pm$ 10 ft about the discrete flight level altitudes assigned by the Air Traffic Control (ATC), specifically over the altitude ranges 33, 34, 35, 36, 37, 38, 39, 40, 41 kft $\pm$ 10 ft. In the ascent and the descent phases, the parameters vary continuously with altitude and are further averaged over intervals of 100 ft to smoothen out the data variation. The Root Sum Squared (RSS) standard deviation is used as the measure of the error in the averaged parameters. All the parameters are expressed as normalized values. The normalization is done with the aim of making the parameters independent of the particular engine type and model.

V.B.   Results

In Figure 2 and Figure 3, the blue line shows the averaged values and the red error bars show one RSS standard deviation about the mean ($\pm 1\sigma$). Although the averaging technique gives discrete parameter

———

American Institute of Aeronautics and Astronautics

values about specific altitudes, the successive points in the plot are joined with straight lines for ease of trend visualization. Figure 2 shows the averaged fuel flow rate and Figure 3 shows the averaged FDR reported thrust as a function of altitude for the different flight phases. These parameters directly control the aircraft emissions. The fuel flow rate is normalized with 2 kg/s, and the FDR reported thrust is normalized with the maximum engine thrust. It should be noted that in the plots for the descent phase, the altitude decreases from left to right as the aircraft comes in for approach.
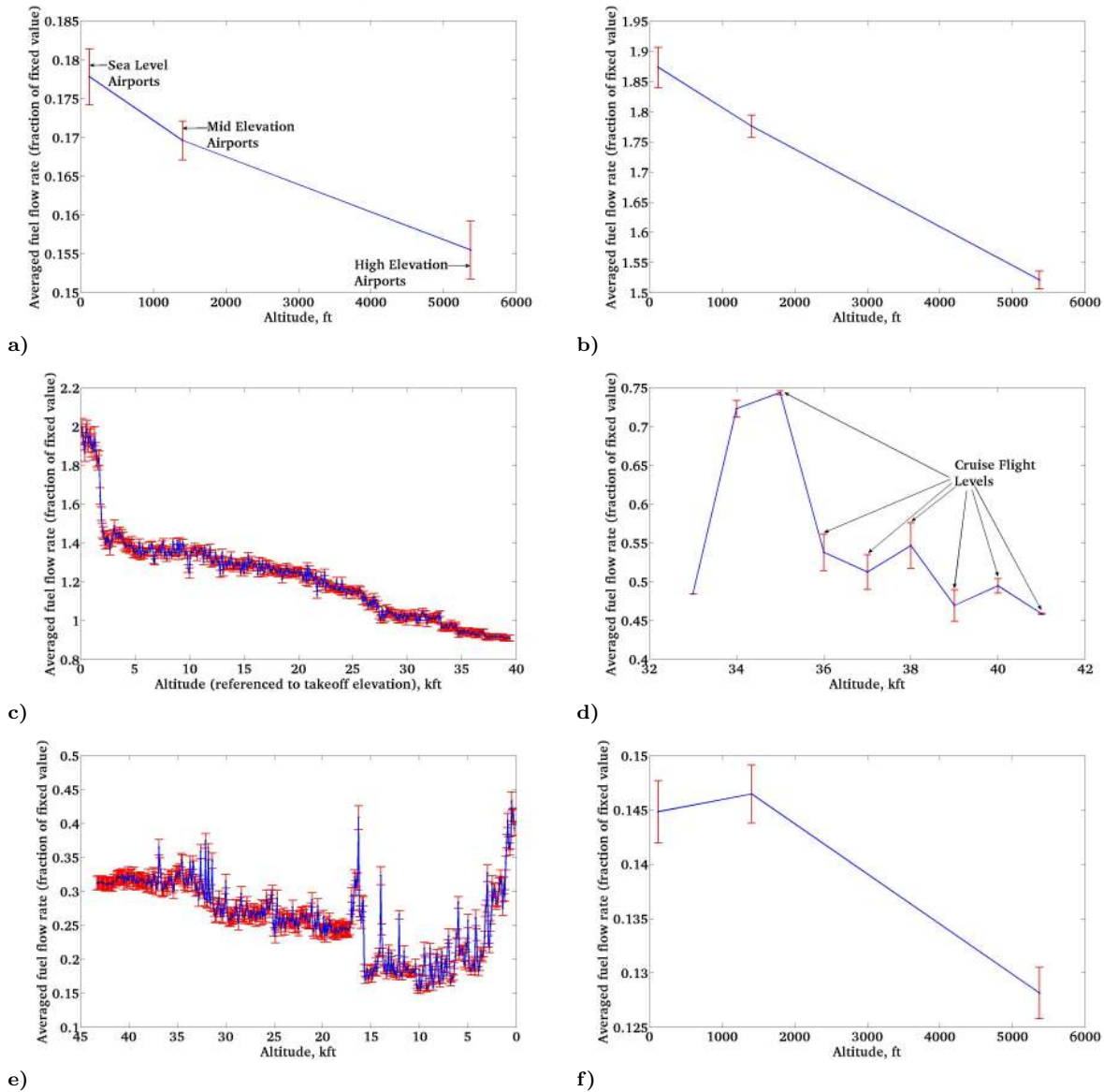

Figure 2. A330 - 223: average normalized fuel flow rate versus pressure altitude; a) departure taxi, b) takeoff, c) ascent, d) cruise, e) descent, and f) arrival roll and taxi

The fuel flow rate and the thrust are seen to follow similar trends, as the fuel flow rate controls the thrust. In the ascent phase, the parameters decrease almost monotonically with altitude. As expected, the thrust (and the fuel flow rate required to generate the thrust) levels in ascent are higher than those in cruise, which in turn are more than those in the initial part of the descent. Close to approach, the thrust (and the fuel flow rate) increases (almost to cruise levels). This is attributed to an increase in drag due to the deployment of auxiliary devices (like spoilers, slats, flaps), and the landing gear. The descent phase shows large fluctuations in engine performance, probably because, unlike ascent, descent is more influenced by ATC procedures.
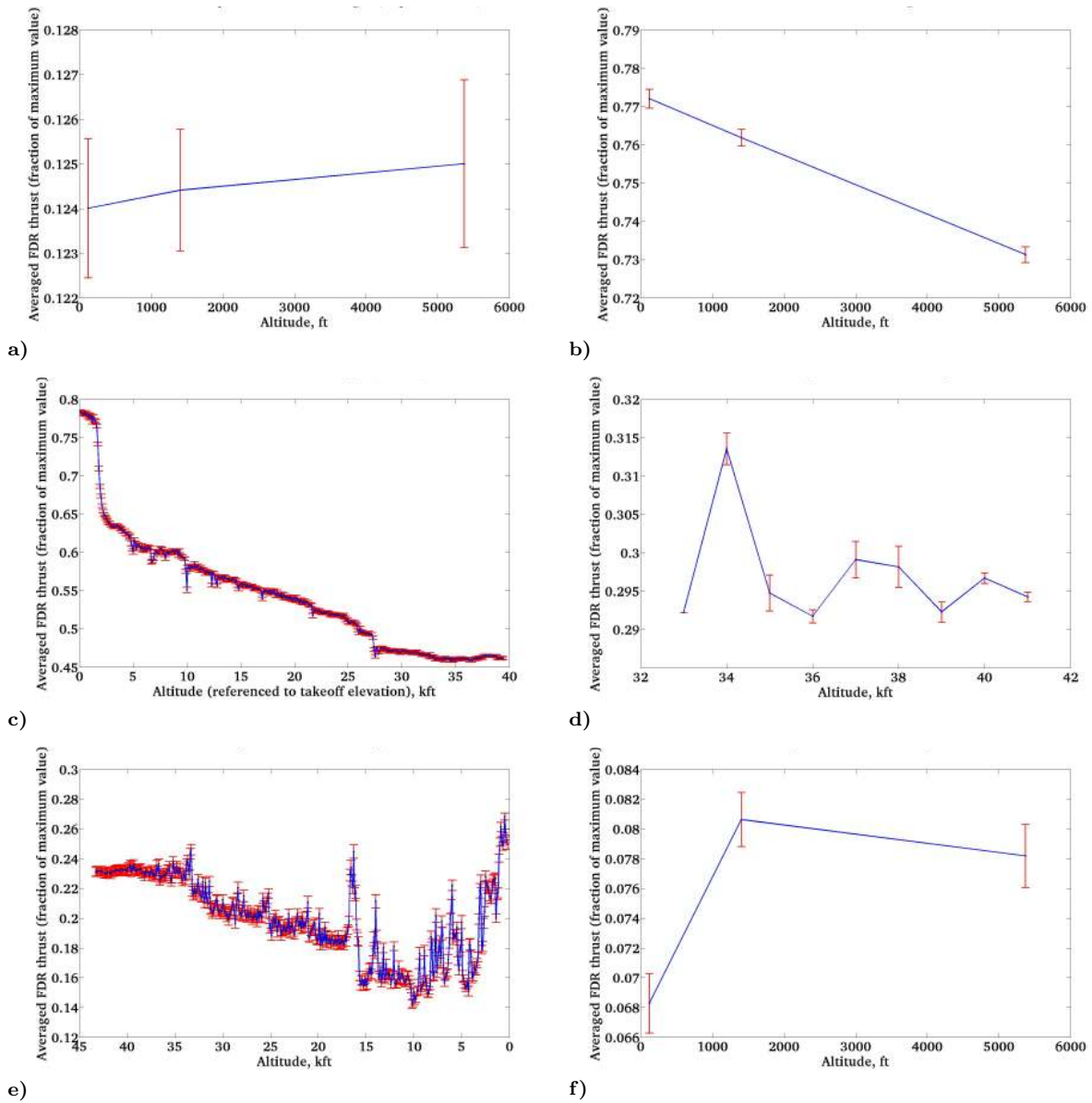
Figure 3. A330 - 223: average normalized FDR reported thrust versus pressure altitude; a) departure taxi, b) takeoff, c) ascent, d) cruise, e) descent, and f) arrival roll and taxi

VI. Modeling of Thrust

VI.A. Methodology

The FDR reported thrust value is believed to be a derived quantity and not a measured one. To understand if the FDR reported thrust data make physical sense, equations for turbofan performance analysis[9] (described in the appendix) are used to calculate the average per engine thrust. The parameters from the FDR data required for the thrust calculation are as follows:

1. Ambient total pressure

2. Ambient total temperature

3. Ambient Mach number

4. Ambient true airspeed

American Institute of Aeronautics and Astronautics

5. Combustor entry pressure

6. Fuel flow rate

7. Engine Pressure Ratio (EPR)

8. Exhaust Gas Temperature (EGT)

The following assumptions are made regarding the aircraft (A330 - 223) and the engine (PW 4168A/4170 turbofan):

1. The wing area of the aircraft is taken to be 361.6 m^2.

2. The engine fan diameter is taken to be 2.54 m.

3. The engine design bypass ratio is taken to be 5.

4. The isentropic efficiences are assumed to be constant 0.88, 0.88 and 0.93 for the fan, compressors, and turbines, respectively. The intake is assumed to have a total pressure loss of 6% (resulting in an Intake total Pressure Ratio, IPR of 0.94) and the combustor is assumed to result in a total pressure loss of 5% (resulting in a Combustor total Pressure Ratio, CPR of 0.95). The nozzles are assumed to be isentropic. These are typical values for engines.

5. In the FDR record, EPR is given as a percentage of its maximum value. The maximum value is taken as 1.75 so that an absolute value for the EPR can be obtained.

6. The ratio of specific heats is assumed to be $\gamma_c = 1.4$ for cold air and $\gamma_h = 1.3$ for the hot mixture of combustion gases. The specific gas constant for air, R, is taken to be 287 Jkg^{-1}K^{-1}.

7. The fuel is assumed to have a Lower Calorific Value (LCV) of 43 MJkg^{-1}.

The net thrust per engine is calculated as the average of the thrusts from both the engines. The thrust is normalized by converting into a fraction of a maximum value. This maximum value is calculated by assuming the fact that the percentage thrust at wheels off is the same for the modeled and the FDR reported thrust. The FDR supplies the value for percentage thrust. It should be noted that most takeoffs are derated and therefore, do not occur at the maximum engine thrust.

VI.B.   Results

Figure 4 shows a very good qualitative agreement between the modeled thrust and the FDR reported thrust. Even small variations are captured quite accurately. This result validates the thrust calculation model and supports the data from the FDR. The agreement is better in those phases of the flight where data acqusition in the FDR occurs more frequently. The agreement is quite inaccurate in the cruise phase where the data are collected every 5 minutes. The quantitative difference between the actual and the modeled values of thrust is attributed to unmodeled effects like installation effects, engine cooling flows, power extraction to run auxiliary devices (like hydraulic, pneumatic, fuel pumps), bleed air extraction, etc. As expected, the thrust levels are the lowest during the taxi phases. The thrust rapidly increases during takeoff, reduces during climb and is fairly constant during cruise. As mentioned before, the thrust levels in ascent are higher than those in cruise, which in turn are more than those in the initial part of the descent. During the descent phase, there is a large fluctuation in the thrust levels which is attributed to ATC procedures coming into play. Towards approach, the thrust increases due to an increase in drag caused by the deployment of spoilers, flaps, slats, and the landing gear. Although Figure 4 shows the results for only one aircraft, similar results are obtained for the other A330 - 223 flights in the study.
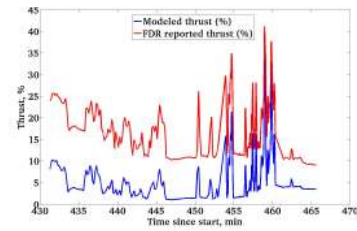
American Institute of Aeronautics and Astronautics
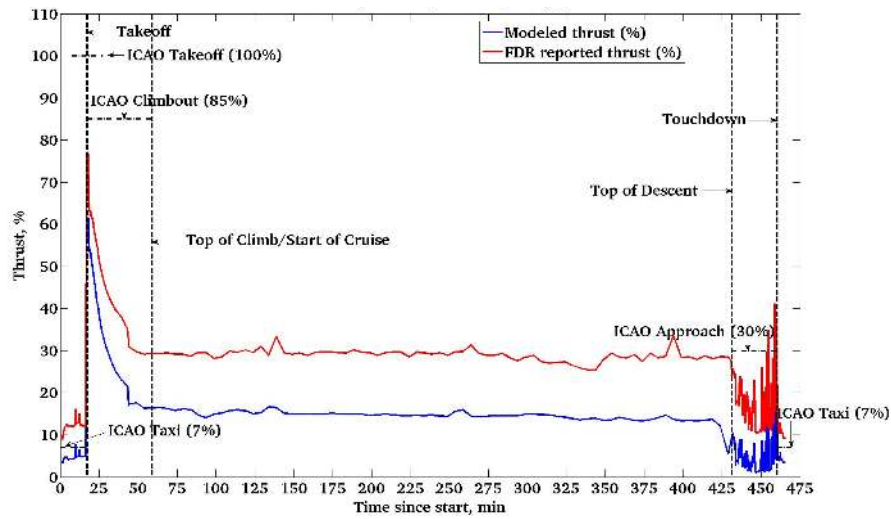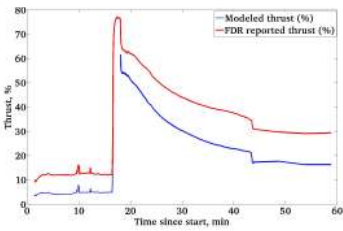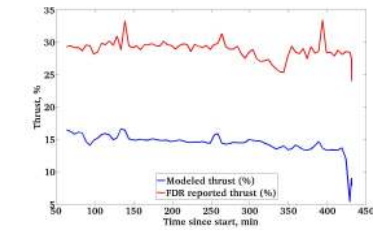
Figure 4. A330 - 223: modeled and FDR reported percentage thrust versus time for a single flight; a) all phases, b) upto top of climb, c) cruise, and d) after top of descent

The good correlation between the modeled and the FDR reported percentage thrusts can also be seen in Figure 5, where data from 54 A330 - 223 flights are plotted together. The scatterplot suggests that it might be possible to estimate the actual operational thrust from the modeled thrust. The percentage thrusts for the different flights are consistent with each other suggesting that the normalization is effective.
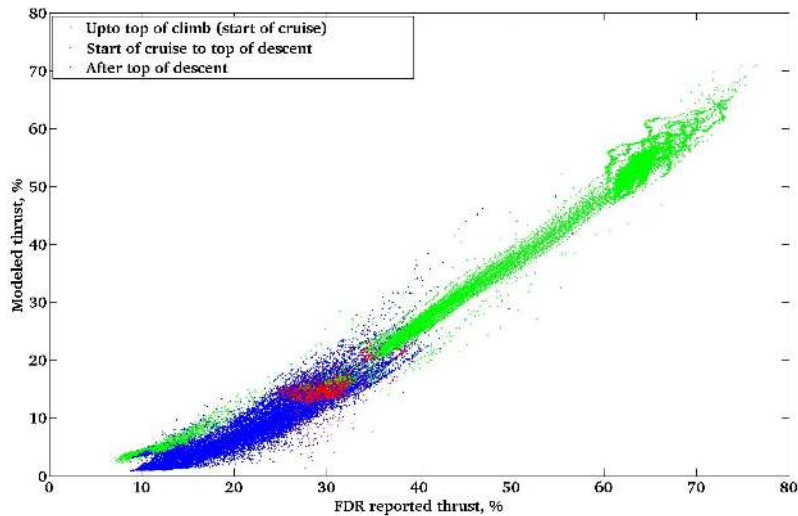

Figure 5. Modeled percentage thrust versus FDR reported percentage thrust (many A330 - 223 flights combined)

American Institute of Aeronautics and Astronautics

VI.C. Comparison with ICAO Standard Values in the LTO Cycle

In Table 2 and Table 3, the operational FDR thrust settings and the times in mode are compared with the ICAO standard values in the Landing and Take Off (LTO) cycle. The values of the operational thrust settings and the times in mode are averaged over the 100 A330 - 223 flights in the study. The operational values are found to differ from the ICAO standard values. Since the ICAO values are used for emissions inventory calculations, this difference reflects the error incurred in fuel burn and emissions estimates. It is important to note that the LTO cycle deals with only that part of the trajectory which is below and upto 3000 ft above the ground level.

Table 2. Percentage thrust settings in the LTO cycle: operational values versus ICAO standard values

	Operational Values (%)	ICAO Values (%)	% Difference
Takeoff	73	100	-27.00
Climbout	72	85	-15.29
Approach	21	30	-30.00
Taxi / Ground Idle	10	7	42.86

Table 3. Times in mode in the LTO cycle: operational values versus ICAO standard values

	Operational Values (s)	ICAO Values (s)	% Difference
Takeoff	41	42	-2.38
Climbout	86	132	-34.85
Approach	233	240	-2.92
Taxi / Ground Idle	1438	1560	-7.82

VII. Conclusions

This paper explores trends in the engine performance data from Flight Data Recorders. There is a significant difference between the actual FDR reported thrust settings and the times in mode and the ICAO standard values in the LTO cycle, which can significantly affect emission inventories. Hence, it is important to be able to model the engine performance as accurately as possible as this accuracy is reflected in the accuracy of aircraft emissions calculations. Future work will subject the FDR data set to different statistical techniques in order to model and predict, for different aircraft and engine types, engine performance, and consequently aircraft emissions, more accurately.

American Institute of Aeronautics and Astronautics

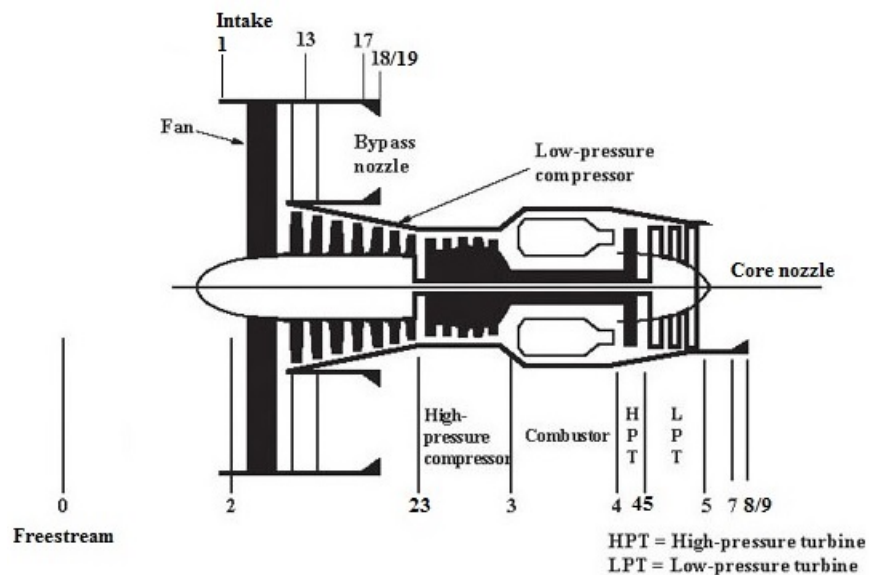# Appendix: Turbofan Performance Analysis Model

Engine Schematic

Figure 6. High bypass unmixed turbofan engine schematic with station numbers[9]

Nomenclature

Station numbers (occurring as subscripts):

0	Freestream
1	Intake face
2	Engine fan face
23	Fan (and Low Pressure Compressor (LPC)) exit (in the core) / High Pressure Compressor (HPC) entry
13	Fan exit (in the bypass)
3	HPC exit / combustor entry
4	Combustor exit / High Pressure Turbine (HPT) entry
45	HPT exit / Low Pressure Turbine (LPT) entry
5	LPT exit
7	Core nozzle entry
8/9	Core nozzle throat / exit
17	Bypass nozzle entry
18/19	Bypass nozzle throat / exit

Roman Symbols:

A	Area
b	Bypass ratio
C_p	Specific heat at constant pressure
CL	Pressure ratio choking limit
CPR	Combustor total Pressure Ratio
EGT	Exhaust Gas Temperature
EPR	Engine total Pressure Ratio
$F_{n,calc}$	Net calculated thrust
f	Fuel to core air mass flow rate ratio

American Institute of Aeronautics and Astronautics

IPR	Intake total Pressure Ratio	
LCV	Lower Calorific Value of the fuel	
M	Mach number	
$\dot{m}$	Mass flow rate	
NPR	Nozzle Pressure Ratio	
P	Pressure	
R	Gas constant for air	
T	Temperature	
V	True velocity	

Greek Symbols:

γ	Ratio of specific heats
η	Isentropic efficiency
π	Total pressure ratio

Subscripts:

a	Core
b	Bypass
c	"Cold" air (not containing the combustion products)
comp	Compresor
f	Fuel
fan	Fan
h	"Hot" air (containing the combustion products)
t	Total
turb	Turbine

Equations

The variables given in the FDR (and hence, used directly) are P_{t0}, T_{t0}, M_0, V_0, P_{t3}, $\dot{m}_f$, EPR, and EGT.

1. *Intake (assumed adiabatic)*

$$P_{t2} = P_{t0} \times IPR \tag{1}$$
$$T_{t2} = T_{t0} \tag{2}$$

2. *Compressor*

$$\pi_{comp} = \frac{P_{t3}}{P_{t2}} \tag{3}$$

$$T_{t3} = T_{t2} + \frac{T_{t2}}{\eta_{comp}} \left(\pi_{comp}^{\frac{\gamma_c - 1}{\gamma_c}} - 1 \right) \tag{4}$$

3. *Turbine*

$$P_{t5} = P_{t2} \times EPR \tag{5}$$
$$T_{t5} = EGT \tag{6}$$
$$\pi_{turb} = \frac{P_{t5}}{P_{t4}} \tag{7}$$
$$T_{t4} = \frac{T_{t5}}{1 - \eta_{turb}\left(1 - \pi_{turb}^{\frac{\gamma_h - 1}{\gamma_h}} \right)} \tag{8}$$

American Institute of Aeronautics and Astronautics

4. *Combustor*

$$P_{t4} = P_{t3} \times CPR \tag{9}$$

$$C_{p_h} = \frac{\gamma_h R}{\gamma_h - 1} \tag{10}$$

$$C_{p_c} = \frac{\gamma_c R}{\gamma_c - 1} \tag{11}$$

$$\dot{m}_a = \frac{\dot{m}_f \left(LCV - C_{p_h} T_{t4} \right)}{C_{p_h} T_{t4} - C_{p_c} T_{t3}} \tag{12}$$

$$f = \frac{\dot{m}_f}{\dot{m}_a} \tag{13}$$

5. *Fan*

$$\dot{m}_b = b\dot{m}_a \tag{14}$$

$$T_{t13} = T_{t2} + \frac{(1+f)\left(T_{t4} - T_{t5} \right) \frac{C_{p_h}}{C_{p_c}} - (T_{t3} - T_{t2})}{b} \tag{15}$$

$$\pi_{fan} = \left(\frac{\eta_{fan} \left(T_{t13} - T_{t2} \right)}{T_{t2}} + 1 \right)^{\frac{\gamma_c}{\gamma_c - 1}} \tag{16}$$

$$P_{t13} = \pi_{fan} P_{t2} \tag{17}$$

6. *Core Nozzle (assumed isentropic and with variable geometry)*

$$P_0 = \frac{P_{t0}}{\left(1 + \frac{\gamma_c - 1}{2} M_0^2 \right)^{\frac{\gamma_c}{\gamma_c - 1}}} \tag{18}$$

$$NPR_a = \frac{P_{t5}}{P_0} \tag{19}$$

$$CL_a = \left(\frac{\gamma_h + 1}{2} \right)^{\frac{\gamma_h}{\gamma_h - 1}} \tag{20}$$

$$M_9 = \begin{cases} \sqrt{\frac{2}{\gamma_h - 1} \left(NPR_a^{\frac{\gamma_h - 1}{\gamma_h}} - 1 \right)} & \text{if } NPR_a < CL_a, \\ 1 & \text{otherwise} \end{cases} \tag{21}$$

$$T_9 = \frac{T_{t5}}{1 + \frac{\gamma_h - 1}{2} M_9^2} \tag{22}$$

$$V_9 = \sqrt{2 C_{p_h} \left(T_{t5} - T_9 \right)} \tag{23}$$

$$P_9 = \frac{P_{t5}}{\left(1 + \frac{\gamma_h - 1}{2} M_9^2 \right)^{\frac{\gamma_h}{\gamma_h - 1}}} \tag{24}$$

$$A_9 = \frac{(1+f)\dot{m}_a \sqrt{\frac{R}{T_{t5}}}}{\sqrt{\gamma_h} P_{t5} M_9 \left(1 + \frac{\gamma_h - 1}{2} M_9^2 \right)^{\frac{-(\gamma_h + 1)}{2(\gamma_h - 1)}}} \tag{25}$$

7. *Bypass Nozzle (assumed isentropic and with variable geometry)*

$$NPR_b = \frac{P_{t13}}{P_0} \tag{26}$$

$$CL_b = \left(\frac{\gamma_c + 1}{2} \right)^{\frac{\gamma_c}{\gamma_c - 1}} \tag{27}$$

American Institute of Aeronautics and Astronautics

$$M_{19} = \begin{cases} \sqrt{\frac{2}{\gamma_c - 1} \left(NPR_b^{\frac{\gamma_c - 1}{\gamma_c}} - 1 \right)} & \text{if } NPR_b < CL_b, \\ 1 & \text{otherwise} \end{cases} \tag{28}$$

$$T_{19} = \frac{T_{t13}}{1 + \frac{\gamma_c - 1}{2} M_{19}^2} \tag{29}$$

$$V_{19} = \sqrt{2 C_{p_c} \left(T_{t13} - T_{19} \right)} \tag{30}$$

$$P_{19} = \frac{P_{t13}}{\left(1 + \frac{\gamma_c - 1}{2} M_{19}^2 \right)^{\frac{\gamma_c}{\gamma_c - 1}}} \tag{31}$$

$$A_{19} = \frac{\dot{m}_b \sqrt{\frac{R}{T_{t13}}}}{\sqrt{\gamma_c} P_{t13} M_{19} \left(1 + \frac{\gamma_c - 1}{2} M_{19}^2 \right)^{\frac{-(\gamma_c + 1)}{2(\gamma_c - 1)}}} \tag{32}$$

8. *Net Calculated Thrust*

$$\begin{aligned} F_{n,calc} = & \; \dot{m}_a \left(1 + f \right) V_9 + \dot{m}_b V_{19} + \left(P_9 - P_0 \right) A_9 + \left(P_{19} - P_0 \right) A_{19} \\ & - \left(\dot{m}_a + \dot{m}_b \right) V_0 \end{aligned} \tag{33}$$

Acknowledgments

References

[1]International Civil Aviation Organization, *ICAO Aircraft Engine Emissions Databank* [online database], URL: http://easa.europa.eu/environment/edb/aircraft-engine-emissions.php [cited 22 July 2013].

[2]Herndon, S. C., Rogers, T., Dunlea, E. J., Jayne, J. T., Miake-Lye, R., and Knighton, B., "Hydrocarbon Emissions from In-Use Commercial Aircraft During Airport Operations," *Environmental Science and Technology*, Vol. 40, No. 14, Jul. 2006, pp. 4406 – 4413.

[3]Herndon, S. C., Wood, E. C., Northway, M. J., Miake-Lye, R., Thornhill, L., Beyersdorf, A., Anderson, B. E., Dowlin, R., Dodds, W., and Knighton, W. B., "Aircraft Hydrocarbon Emissions at Oakland International Airport," *Environmental Science and Technology*, Vol. 43, No. 6, Feb. 2009, pp. 1730 – 1736.

[4]Trani, A. A., Wing - Ho, F. C., Schilling, G., Baik, H., and Seshadri, A., "A Neural Network Model to Estimate Aircraft Fuel Consumption," *AIAA 4th Aviation Technology, Integration and Operations (ATIO) Forum*, Chicago, Illinois, 2004.

[5]Collins, B. P., "Estimation of Aircraft Fuel Consumption," *AIAA Journal of Aircraft*, Vol. 19, No. 11, Nov. 1982, pp. 969 – 975.

[6]Yoder, T., "Development of Aircraft Fuel Burn Modeling Techniques with Applications to Global Emissions Modeling and Assessment of the Benefits of Reduced Vertical Separation Minimums," S.M. Thesis, Department of Aeronautics and Astronautics, Massachusetts Institute of Technology, Cambridge, MA, Jun. 2007.

[7]Khadilkar, H., and Balakrishnan, H., "Estimation of Aircraft Taxi Fuel Burn Using Flight Data Recorder Archives," *Transportation Research Part D*, Vol. 17, No. 7, Oct. 2012, pp. 532 – 537.

[8]Patterson, J., Noel, G. J., Senzig, D. A., Roof, C. J., and Fleming, G. G., "Analysis of Departure and Arrival Profiles Using Real-Time Aircraft Data," *AIAA Journal of Aircraft*, Vol. 46, No. 4, Jul. 2009, pp. 1094 – 1103.

[9]Cumpsty, N. A., *Jet Propulsion: A Simple Guide to the Aerodynamics and Thermodynamic Design and Performance of Jet Engines*, 2nd ed., Cambridge University Press, Cambridge, U.K., 2003, Chaps. 1 – 10.